Carrier Transport in a Two-Dimensional Topological Insulator Nanoribbon in the Presence of Vacancy Defects.

Sabyasachi Tiwari[1], Maarten L. Van de Put[1], Bart Sorée[2], and William G. Vandenberghe[1]
[1]*Department of Materials Science and Engineering, The University of Texas at Dallas, 800 W. Campbell Rd., Richardson, Texas 75080, USA.*
[2]*Imec, Kapeldreef 75, 3001 Heverlee, Belgium; Department of Electrical Engineering, KU Leuven, Naamsestraat 63, 3000 Leuven, Belgium; Department of Physics, Universiteit Antwerpen, Prinsstraat 13, 2000 Antwerp, Belgium.*

***Abstract*—We model transport through two-dimensional topological insulator (TI) nanoribbons. To model the quantum transport, we employ the non-equilibrium Green's function approach. With the presented approach, we study the effect of lattice imperfections on the carrier transport. We observe that the topologically protected edge states of TIs are robust against a high percentage (2%) of vacancy defects. We also investigate tunneling of the edge states in two decoupled TI nanoribbons.**

I. Introduction

To continue the scaling of electronic devices, the use of two-dimensional (2D) materials becomes indispensable for maintaining optimum electrostatic control [1]. A range of 2D materials have been investigated since the advent of graphene [2]. Intrinsic material properties of 2D materials like silicene, germanene [3], phosphorene [4] and transition-metal dichalcogenides [5] have been investigated extensively, along with their possible use as a channel material for field-effect transistors (FETs) [6]. However, one of the major problems one encounters with these 2D materials is the abundance of defects [7], mostly vacancy defects [8]. Vacancies in the channel material can deteriorate the performance of the transistor in terms of speed of operation. Recently, transistors using TI nanoribbons as channel material have been proposed [9], the so-called Topological Insulator FETs (TIFETs). The switching mechanism of these TIFETs is based on the modulation of scattering.

Two-dimensional topological insulators are a class of 2D materials with conducting metallic edge states in their ribbon form. The edge states are protected by time-reversal symmetry and time-reversal symmetry conserving perturbations (e.g vacancies) cannot back-scatter carriers traveling through these conducting edge states. The edge states that travel in the same/opposite direction, but with opposite/same spin are located on opposite edges. Therefore, to change the direction of motion ($k_{\mathrm{x}} \rightarrow -k_{\mathrm{x}}$), the edge states have to either flip their spin or change to the opposite edge (inter-edge scattering). Scattering on vacancies can not introduce spin flipping [10]. However, a high percentage of vacancy defects can facilitate back-scattering of the edge states by augmenting inter-edge interactions [11].

To quantify this effect, we study the impact of vacancy defects on the carrier transport of a TI nanoribbon using the non-equilibrium Green's function approach. The electronic structure of TIs is modeled using the Kane-Mele Hamiltonian [12]. Also, we qualitatively show how the presence of vacancy defects can result to a better ON-OFF characteristic of the TIFETs.

In section II, we decribe the methodology. In section III, we describe the obtained results and in section IV, we conclude.

II. Methodology

To model the electronic structure of the 2D TI nanoribbon, we use the Kane-Mele tight-binding Hamiltonian for a hexagonal lattice [12],

$$H = -t \sum_{\langle i,j\rangle,\alpha} c^{\dagger}_{i,\alpha} c_{j,\alpha} + i\Lambda_{\mathrm{so}} \sum_{\langle\langle i,j\rangle\rangle,\alpha,\beta} v_{i,j} c^{\dagger}_{i,\alpha} \sigma^{z}_{\alpha,\beta} c_{j,\beta} + i\Lambda_{\mathrm{R}} \sum_{\langle i,j\rangle,\alpha,\beta} c^{\dagger}_{i,\alpha} (\sigma \times \hat{d_{i,j}})^{z}_{\alpha,\beta} c_{j,\beta}, \tag{1}$$

where the first term describes the nearest-neighbour hopping with coupling strength t and $c^{\dagger}_{i,\alpha}$, $c_{j,\alpha}$ as creation and annihilation operators at sites i and j and components ($\alpha \in \{\uparrow,\downarrow\}$). The second term describes the next nearest neighbour hopping with spin-orbit interaction, with $i\Lambda_{\mathrm{so}}$ as the spin-orbit coupling, $v_{i,j} = +1$ for $i \rightarrow j$ and -1 for $j \rightarrow i$ hopping, $\beta \in \{\uparrow,\downarrow\}$ and $\sigma^{z}_{\alpha,\beta}$ is the indicated Pauli matrix. The third term describes the Rashba spin-orbit coupling between nearest neighbour sites. The Rashba term specifically breaks the ($z \rightarrow -z$) out-of-plane symmetry under the influence of a perpendicular electric field or interaction with the substrate. Since we do not consider any substrate interaction or perpendicular electric field, we can safely neglect the Rashba (Λ_{R}) term.

The parameters used for the simulation of TI nanoribbons are obtained by fitting the low energy band structure (obtained by diagonalizing the Kane-Mele Hamiltonian) with the band structure of Stanene obtained from DFT as implemented in the Vienna Ab Initio Simulation Package (VASP) [13] [14] ($t = 0.85\mathrm{eV}$, $\Lambda_{\mathrm{so}} = 0.01\mathrm{eV}$). Stanene is a 2D Topological Insulator [15].
Vacancy defects are modeled by replacing the local atomic contribution to the Hamiltonian with the vacuum Hamiltonian of the form,

$$H_{\mathrm{v}} = V_0 \sum_{\mathrm{R},\alpha} c^{\dagger}_{\mathrm{R},\alpha} c_{\mathrm{R},\alpha} + t_{\mathrm{l}} \sum_{\langle \mathrm{R,r}\rangle,\alpha} c^{\dagger}_{\mathrm{R},\alpha} c_{\mathrm{r},\alpha}, \tag{2}$$

978-1-5386-6790-3/18/$31.00 ©2018 IEEE

where 'R' is the lattice site where the vacancy defect is present, α is the spin, t_l is the coupling strength between the vacancy site 'R' and its nearest-neighbour lattice site 'r', and V_0 is the onsite potential. The onsite potential (V_0) for vacancies has been set to 24.5 eV. The coupling coefficient (t_l) has been set to 0.51 eV.

To investigate the flow of carriers in a finitely sized 2D TI nanoribbon, we employ the non-equilibrium Green's function formalism [16]. Within this formalism, we calculate the retarded Green's function $G^{\mathrm{r}}(E)$ and the advanced Green's function $G^{\mathrm{a}}(E)$ as,

$$G^{\mathrm{r}}(E) = (EI - H - \Sigma_{\mathrm{R}}(E) - \Sigma_{\mathrm{L}}(E))^{-1}, \tag{3a}$$

$$G^{\mathrm{a}}(E) = (G^{\mathrm{r}}(E))^{\dagger}, \tag{3b}$$

where $\Sigma_{\mathrm{R}}(E)$, $\Sigma_{\mathrm{L}}(E)$ are the respective right and left contact self-energies that describe the open boundary conditions with infinite leads. We use the quantum transmitting boundary method (QTBM) [17] to calculate the contact self-energies. In order to obtain the solution for the lead wave functions, we use the periodic boundary condition at the left/right lead and expand the tight-binding Hamiltonian for energy E as,

$$(W_{-}\lambda^2 + H_0\lambda + W_{+})\phi_{\mathrm{L/R}} = E\lambda\phi_{\mathrm{L/R}}. \tag{4}$$

Here, $\phi_{\mathrm{L/R}}$ is the wave function. W_{-} is the hopping matrix for the unit cell block on the left side and W_{+} for the right side of the lead unit cell, $\lambda = \exp(-ik\Delta a)$, where i is the imaginary unit, Δa is the lattice constant and k is the wave-vector. H_0 is the onsite matrix block. Linearizing the quadratic eigenvalue problem, we obtain,

$$\begin{bmatrix} 0 & I \\ -W_{+} & EI - H_0 \end{bmatrix} \begin{bmatrix} \phi_{\mathrm{L/R}} \\ \lambda\phi_{\mathrm{L/R}} \end{bmatrix} = \lambda \begin{bmatrix} I & 0 \\ 0 & W_{-} \end{bmatrix} \begin{bmatrix} \phi_{\mathrm{L/R}} \\ \lambda\phi_{\mathrm{L/R}} \end{bmatrix}. \tag{5}$$

The resulting generalized eigenvalue equation is diagonalized, resulting in the eigenvalues λ. We distinguish between three cases with $|\lambda| = 1$, $|\lambda| > 1$ and $|\lambda| < 1$. Solutions, where $|\lambda| \leq 1$, correspond to traveling and evanescent modes that are non- divergent in the leads. Hence, we filter out modes within the unit circle $|\lambda| \leq 1$. These solutions ($|\lambda| \leq 1$) contains both traveling and evanescent modes. To build the self-energies, we select only those traveling modes with group velocities that indicate flow into the leads. The group velocity is determined using the Hellman-Feynman technique [18]. In Fig. 1, we show the bandstructure calculated from the traveling modes in the pristine TI nanoribbon lead.

From the eigenvalues (λ) and the eigenvectors ($\phi_{\mathrm{L/R}}$) of the selected modes in each lead, we calculate the self-energy matrices as,

$$\Sigma_{\mathrm{L/R}} = W_{-}\Phi_{\mathrm{L/R}}\Lambda\Phi^{-1}_{\mathrm{L/R}}, \tag{6}$$

where $\Phi_{\mathrm{L/R}}$ is a matrix whose columns comprise the wave functions $\phi_{\mathrm{L/R}}$. Λ is a diagonal matrix comprising of the eigenvalues obtained as λ. From the obtained value of the self-energies, the contact broadning matrices can be calculated as $\Gamma_{\mathrm{R/L}} = i[\Sigma_{\mathrm{R/L}} - \Sigma_{\mathrm{R/L}}{}^{\dagger}]$ and the transmission function as,

$$T(E) = \mathrm{Tr}(\Gamma_{\mathrm{L}}G^{\mathrm{r}}\Gamma_{\mathrm{R}}G^{\mathrm{a}}). \tag{7}$$

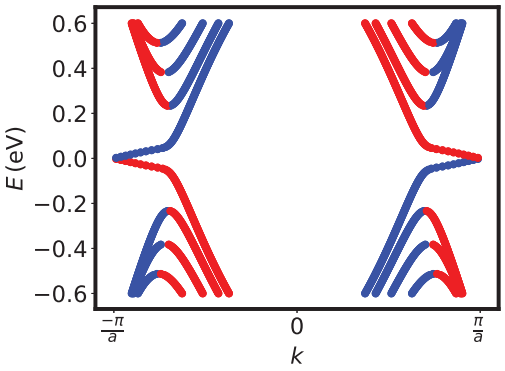

Fig. 1: Bandstructure of the 6.28 nm wide nanoribbon obtained using the QTBM procedure as explained in the text. Blue dots show electrons moving in the positive sense, while red dots show electrons moving in the negative sense.

The spectral function can be written as,

$$A_{\mathrm{L/R}}(E) = G^{\mathrm{r}}\Gamma_{\mathrm{L/R}}G^{\mathrm{a}}, \tag{8}$$

which represents the local density of states (LDOS) at energy E. To further investigate the transport in a 2D TI nanoribbon, we calculate the local current density for an applied bias of $\Delta V = \mu_{\mathrm{L}} - \mu_{\mathrm{R}}$. Where, $\mu_{\mathrm{L/R}}$ are the left and right chemical potentials. The local current density between sites 'i' and 'j' at an energy E is given as,

$$I_{i,j}(E) = -\frac{q}{\hbar}\mathrm{Im}(G^{<}_{i,j}H_{i,j} - G^{<}_{j,i}H_{j,i}), \tag{9}$$

where q is the electron charge and $G^{<}_{i,j}$ is the lesser Green's function between sites 'i' and 'j' at energy E. The lesser Green's function ($G^{<}_{i,j}$) can be calculated as,

$$G^{<}_{i,j} = A_{\mathrm{L}}f(E - \mu_{\mathrm{L}}) + A_{\mathrm{R}}f(E - \mu_{\mathrm{R}}), \tag{10}$$

where $f(E)$ is the Fermi-Dirac distribution at room temperature.

III. Results and Discussion

With the methodology described in the previous section, we simulate a 2D TI-nanoribbon with a hexagonal lattice structure and a zigzag edge, as illustrated in Fig. 2(a). The transmission of the pristine ribbon is shown in Fig. 2(b), where we can see that the edge states have a transmission equal to 2. By linearizing the Kane-Mele Hamiltonian around high symmetry point 'K', the energy band gap is found to be $6\sqrt{3}\Lambda_{\mathrm{so}}$. For the parameters chosen for stanene, this value equals 0.1 eV. Therefore, the edge states exist only within the energy window of $\pm$0.05 eV, as shown in Fig. 2(b).

Fig. 3(a) shows the spectral function calculated at an energy 0 eV, which corresponds to an edge state. We observe the exponential localization of the edge states at the two edges of the ribbon, because we only injected states from the left contact, the edge states have opposite spin. We further calculate the local current for the edge states at energy 0 eV

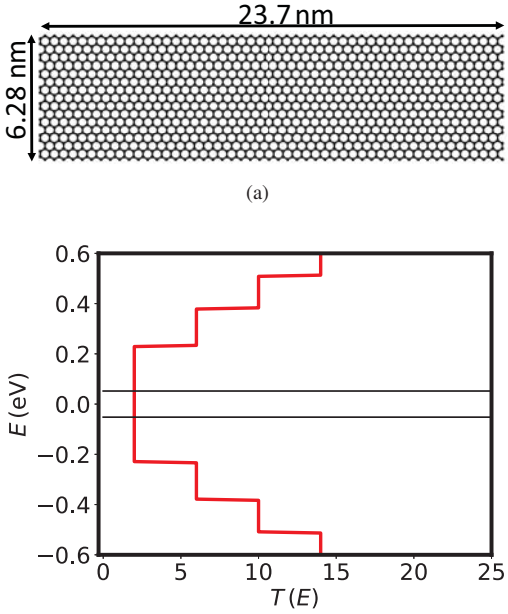

Fig. 2: (a) An illustration of a pristine TI nanoribbon. (b) The calculated transmission for the ribbon shown in (a). We can see that the transmission for the edge states (between the black lines) reaches the expected value 2.

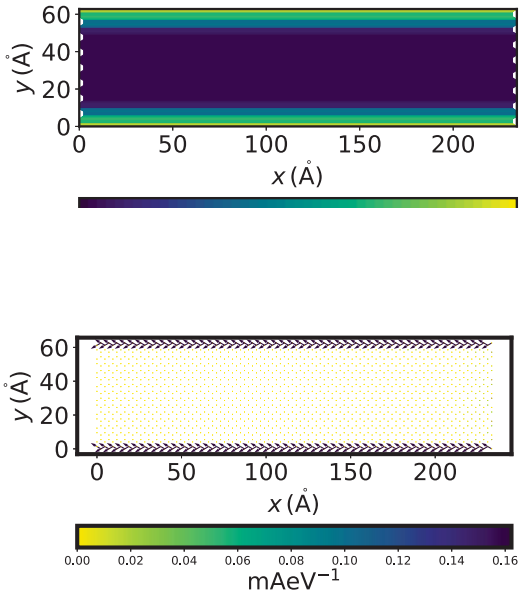

Fig. 3: (a) The spectral function for a pristine ribbon calculated at energy 0 eV which corresponds to an edge state. We can see the localized edge states. (b) Shows the local current calculated at energy 0 eV with an injection from the left side. We can see that the edge state current is localized and unidirectional.

and project it on the hexagonal lattice structure. As expected, the edge states move in one direction as shown in Fig. 3(b).

Now, we add vacancy defects in the pristine TI lattice. Fig. 4(b) shows the effect of a random distribution of vacancy defects on theTI nanoribbons. We have considered 50 different configurations for each defect density and have calculated their mean transmission as well as their standard deviation. It can be inferred from Fig. 4(b) that the edge states of TI nanoribbons maintain their transmission even at a defect density as high as 2%. However, the bulk state transmission drops significantly in the presence of vacancy defects. The drop in transmission coefficient of the bulk states will lead towards a degraded current if the Fermi level is in the bulk state energy range. However, if the Fermi level resides within the edge state energy range then the current drop is insignificant. Previously, TI-transistors that operate on scattering-based switching have been proposed using 2D-TIs [9]. The proposed switching method involves pushing the Fermi level into the bulk states from the edge states to enhance the dissipative scattering process with imperfections. Our results indicate that the scattering role can also be fulfilled by coherent scattering on vacancies.

We extend the application of our method from random defects to ordered nanostructures of TI nanoribbons as shown in Fig. 5(a). The motivation to study such a structured ribbon comes from the fact that the edge states will not be back-scattered. Hence, a change in the ribbon shape should not affect the edge state transmission, whereas bulk states would be reflected significantly, given the right structure. Due to this,

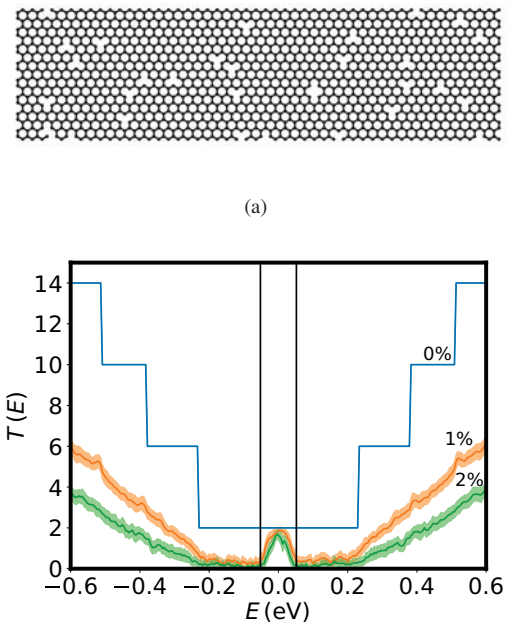

Fig. 4: (a) An illustration of a TI nanoribbon sample with a random defect density of 2%. (b) A comparison of the transmission for a defect density of 0%, 1% and 2%.

the bulk state transmission would fall. From the transmission coefficient in Fig. 5(b), we observe that the topological edge

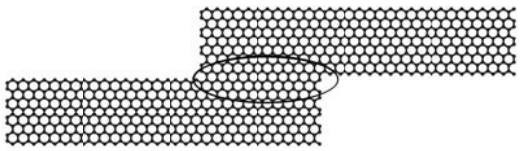

(a)

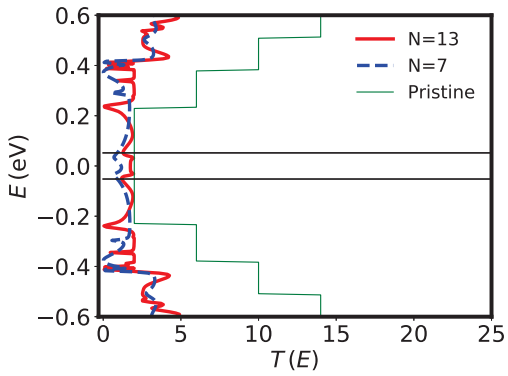

(b)

Fig. 5: (a) An illustration of a structured TI nanoribbon. (b) A comparison of the transmission for a cross-section (encircled) of 13 and 7 atoms (N) in the overlap region with that of a pristine straight ribbon. The edge states maintain their transmission for N=13 but bulk states show a significant drop compared to the pristine ribbon. When N=7, transmission of the edge states falls due to inter-edge back-scattering.

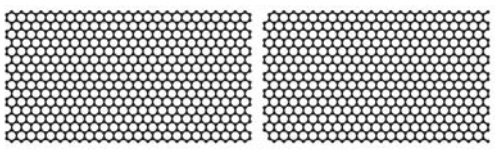

(a)

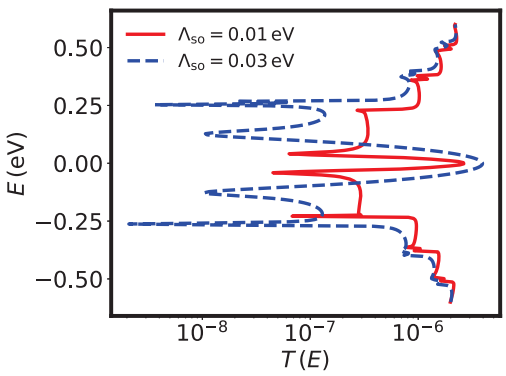

(b)

Fig. 6: (a) An illustration of two decoupled ribbons. (b) A comparison of the transmission for different values of the spin-orbit coupling parameter (Λ_{so}). We see that the tunneling probability increases with an increase in Λ_{so}

states maintain a similar transmission as in a straight ribbon while the bulk state transmission drops significantly, as expected. However, when the overlap between the two regions is narrowed to a range of the order of the decay length of edge state wave functions, significant reflection of the edge states also occurs. This happens due to the inter-edge interaction as discussed previously.

Finally, we study the tunneling properties between two decoupled TI-nanoribbons as shown in Fig. 6(a). In Fig. 6(b), we see that this structure features a sharp peak in the transmission around the Dirac point, indicating tunneling of the topologically protected edge states. To further understand the process, we compare two ribbons with different spin-orbit coupling parameters ($\Lambda_{so} = 0.01$eV and $\Lambda_{so} = 0.03$eV). A coupling of $\Lambda_{so} = 0.03$eV leads to a band gap of 0.31 eV, which is close to the energy band gap of functionalized stanene [19]. From the Fig. 6(b), we see that the edge state tunneling increases with increasing spin-orbit coupling. We attribute this effect to the increased localization of the wave function at the edges with increasing spin-orbit coupling.

IV. Conclusion

We have simulated transport through 2D TI-nanoribbons with a hexagonal lattice structure and zigzag edges using the non-equilibrium Green's function formalism. We have studied the effect of vacancy defects on the transport of carriers through TI nanoribbons. We have found that the topologically protected edge states of 2D-TI nanoribbons are immune to vacancy defects to a large extent, while the bulk states are severely affected. This ensures that TIFETs based on TI ribbons with a high defect density would maintain their high ON current and a low off-state current, without even considering additional incoherent scattering. We have also simulated nanostructured ribbons to study the effect of inter-edge interaction and the tunneling process. We have studied the limits of the robustness of TI-edge states in terms of transmission and have observed that the TI nanoribbons do maintain their transmission when the inter-edge distance is higher than the decay length of their wave functions. Finally, we have observed that the tunneling process between decoupled TI nanoribbons is characterized by a sharp peak in the transmission around the Dirac point.

V. Acknowledgement

This material is based in part upon the work supported by the National Science Foundation under Grant Number 1710066.

The project or effort depicted was or is sponsored by the Department of the Defense, Defense Threat Reduction Agency. The content of the information does not necessarily reflect the position or the policy of the federal government, and no official endorsement should be inferred.

REFERENCES

[1] M. V. Fischetti, B. Fu, and W. G. Vandenberghe, "Theoretical study of the gate leakage current in sub-10-nm field-effect transistors," *IEEE Transactions on Electron Devices*, vol. 60, no. 11, pp. 3862–3869, Nov 2013.

[2] K. S. Novoselov, A. K. Geim, S. V. Morozov, D. Jiang, Y. Zhang, S. V. Dubonos, I. V. Grigorieva, and A. A. Firsov, "Electric field effect in atomically thin carbon films," *Science*, vol. 306, no. 5696, pp. 666–669, 2004.

[3] M. Houssa, E. Scalise, K. Sankaran, G. Pourtois, V. V. Afanasev, and A. Stesmans, "Electronic properties of hydrogenated silicene and germanene," *Applied Physics Letters*, vol. 98, no. 22, p. 223107, 2011.

[4] H. Liu, A. T. Neal, Z. Zhu, Z. Luo, X. Xu, D. Tománek, and P. D. Ye, "Phosphorene: An unexplored 2d semiconductor with a high hole mobility," *ACS Nano*, vol. 8, no. 4, pp. 4033–4041, Apr 2014.

[5] Q. H. Wang, K. Kalantar-Zadeh, A. Kis, J. N. Coleman, and M. S. Strano, "Electronics and optoelectronics of two-dimensional transition metal dichalcogenides," *Nature Nanotechnology*, vol. 7, pp. 699 EP –, Nov 2012, review Article.

[6] V. Podzorov, M. E. Gershenson, C. Kloc, R. Zeis, and E. Bucher, "High-mobility field-effect transistors based on transition metal dichalcogenides," *Applied Physics Letters*, vol. 84, no. 17, pp. 3301–3303, 2004.

[7] S. McDonnell, R. Addou, C. Buie, R. M. Wallace, and C. L. Hinkle, "Defect-dominated doping and contact resistance in mos2," *ACS Nano*, vol. 8, no. 3, pp. 2880–2888, Mar 2014.

[8] Z. Lin, B. R. Carvalho, E. Kahn, R. Lv, R. Rao, H. Terrones, M. A. Pimenta, and M. Terrones, "Defect engineering of two-dimensional transition metal dichalcogenides," *2D Materials*, vol. 3, no. 2, p. 022002, 2016.

[9] W. G. Vandenberghe and M. V. Fischetti, "Imperfect two-dimensional topological insulator field-effect transistors," *Nature Communications*, vol. 8, pp. 14 184 EP –, Jan 2017, article.

[10] J. S. Van Dyke and D. K. Morr, "Effects of defects and dephasing on charge and spin currents in two-dimensional topological insulators," *Phys. Rev. B*, vol. 95, p. 045151, Jan 2017.

[11] X. Dang, J. D. Burton, and E. Y. Tsymbal, "Local currents in a 2d topological insulator," *Journal of Physics: Condensed Matter*, vol. 27, no. 50, p. 505301, 2015.

[12] C. L. Kane and E. J. Mele, "Z_2 topological order and the quantum spin hall effect," *Phys. Rev. Lett.*, vol. 95, p. 146802, Sep 2005.

[13] G. Kresse and J. Furthmüller, "Efficient iterative schemes for ab initio total-energy calculations using a plane-wave basis set," *Phys. Rev. B*, vol. 54, pp. 11 169–11 186, Oct 1996.

[14] P. E. Blöchl, "Projector augmented-wave method," *Phys. Rev. B*, vol. 50, pp. 17 953–17 979, Dec 1994.

[15] Y. Xu, B. Yan, H.-J. Zhang, J. Wang, G. Xu, P. Tang, W. Duan, and S.-C. Zhang, "Large-gap quantum spin hall insulators in tin films," *Phys. Rev. Lett.*, vol. 111, p. 136804, Sep 2013.

[16] R. Lake, G. Klimeck, R. C. Bowen, and D. Jovanovic, "Single and multiband modeling of quantum electron transport through layered semiconductor devices," *Journal of Applied Physics*, vol. 81, no. 12, pp. 7845–7869, 1997.

[17] C. S. Lent and D. J. Kirkner, "The quantum transmitting boundary method," *Journal of Applied Physics*, vol. 67, no. 10, pp. 6353–6359, 1990.

[18] R. P. Feynman, "Forces in molecules," *Phys. Rev.*, vol. 56, pp. 340–343, Aug 1939.

[19] A. Suarez Negreira, W. G. Vandenberghe, and M. V. Fischetti, "Ab initio study of the electronic properties and thermodynamic stability of supported and functionalized two-dimensional sn films," *Phys. Rev. B*, vol. 91, p. 245103, Jun 2015.